Journal Pre-proofs

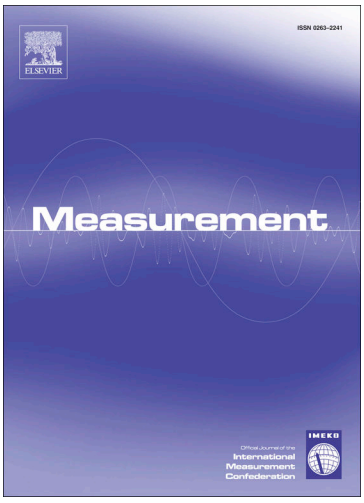

Real-time displacement monitoring using camera video records with camera motion correction

Zhuoran Yi, Miao Cao, Yuya Kito, Gota Sato, Xuan Zhang, Liyu Xie, Songtao Xue

PII: S0263-2241(24)00291-4
DOI: https://doi.org/10.1016/j.measurement.2024.114406
Reference: MEASUR 114406

To appear in: *Measurement*

Received Date: 30 December 2023
Revised Date: 7 February 2024
Accepted Date: 27 February 2024

Please cite this article as: Z. Yi, M. Cao, Y. Kito, G. Sato, X. Zhang, L. Xie, S. Xue, Real-time displacement monitoring using camera video records with camera motion correction, *Measurement* (2024), doi: https://doi.org/10.1016/j.measurement.2024.114406

Real-time Displacement Monitoring Using Camera Video Records with Camera Motion Correction

Zhuoran Yi [a], Miao Cao [b], Yuya Kito [b], Gota Sato [b], Xuan Zhang [b,c],

Liyu Xie [a], Songtao Xue [a,b]*

[a] Department of Disaster Mitigation for Structures, Tongji University, 200092, Shanghai, China

[b] Department of Architecture, Tohoku Institute of Technology, 982-8577, Sendai, Japan

[c] College of Engineering and Architecture, Shandong University of Science and Technology, 266590, Qingdao, China

Email of each authors: Zhuoran Yi linsmyk@gmail.com; Miao Cao caomiao@tohtech.ac.jp;

Yuya Kito m223807@st.tohtech.ac.jp; Gota Sato m223811@st.tohtech.ac.jp ;

Xuan Zhang zhangxuan12341234@163.com; Liyu Xie liyuxie@tongji.edu.cn;

Songtao Xue xuest@tohtech.ac.jp;

* Corresponding author: Songtao Xue

E-mail address: xuest@tohtech.ac.jp

Real-time Displacement Monitoring Using Camera Video Records with Camera Motion Correction

Abstract: Structure from Motion (SfM) method can reconstruct the story drift ratio, but the camera motion produced by earthquakes reduces the measuring accuracy. This paper improves the applicability of the traditional method by correcting camera motion according to the identification of translation and rotation of camera. Experiments at different levels are designed to prove the proposed method. First, one set of experiments proves the motion correction method by the Single-degree-of-freedom (SDOF) system.

The error of maximum response is 4.5% for the case with less rotation. As for the camera motion with larger rotation, the average error increases to 7.9%, which still meets the practical utilization. After that, the accuracy of using SfM method is confirmed by the Multi-degree-of-freedom (MDOF) system with the average error of 4.9%. This paper is expected to extend approaches for the application of the SfM method in the case of huge earthquakes.

Keywords: Story drift; SHM system; Structure from Motion; Camera motion correction; Shaking table test;

1. Introduction

Maximum story drifts of a structure during an earthquake are significant to identifying the damage level and remaining seismic capacity [1,2]. By contrast, drift measurement remains a problem [3–5]. There are mainly two ways to obtain story drifts. One way works directly by attached sensors based on inductive difference [6–8], laser [9–11], Fiber Bragg Grating (FBG) [12-14], or Linear Variable Differential Transformer (LVDT) [15-16]. These sensors are capable of displacement sensing, while installation will be a huge problem due to the requirement of reference points, especially when applied to real structures. Another way is to reconstruct displacement indirectly according to the acceleration data, such as integration [17–18], numerical models [19-20], or Bayesian-based methods [21-22]. Nevertheless, the accuracy is highly related to the original settings, hence showing considerable error when the settings differ from real conditions.

Considering above shortcomings, researchers expect to observe real-time drifts directly by the image identification of videos taken during earthquakes. Compared with other visual-based technology, Structure from Motion(SfM) method has proven to be a potential tool for reconstructing drifts due to the low requirements of reference points, especially for the 3D reconstruction with an unknown camera position [23]. Several SfM-based techniques have been proposed under different assumptions of camera motion: 1). Ignore camera motion. Cameras are assumed to be constant during detection [24-26], which is not capable for drift monitoring during earthquakes. 2). Correct camera motion in the meantime. This research has just begun several years ago. Camera motion will be estimated and utilized for calibration of identified structural drift [27-28]. Several problems exist in recent work. On the one hand, some work did not correct rotation [27], which limited the utilization under huge earthquakes. On the other hand, the reference points were mainly identified from the rigid feature [28], which cost larger calculations and may increase the error when the image distortion happens under huge earthquakes. When drift detection under possible huge earthquakes is considered, these two problems should be discussed.

Another problem is related to the experiments for feasibility verification. The characteristics of the experiments reported recently have been summarized as follows:

1). Only simulation is utilized to confirm the feasibility of the proposed method [29].

2). The structure or member has no vibration [27, 29, 30].

3). Only the translation is considered [27]. The camera has no rotation.

4) Only the translation and slight rotation of the camera are considered. The camera motion is introduced by a shaking table. The rotation is aroused because of the translation [28].

It should be noted that the influence of rotation has been underestimated in recent experiments of the camera motion correction for the SfM-based method. Since a huge earthquake will give a rather random motion to the camera, which includes not only translation but also considerable rotation, an experiment containing both rotation and translation of the camera is needed to verify the feasibility of the proposed method.

This paper has proposed an image identification method for drift detection with the correction of camera motion in the meantime. Reference points are directly obtained from several attached square markers at the surface of the target structure rather than identifying the rigid feature. In each time step, the camera's translation and rotation (both in and out of the plane) will be identified by comparing the coordinates of reference points and solving the projection equation further. Then, the SfM method has been selected to obtain the structural drift from the revised image. Experiments with fewer or larger camera rotations are carried out to prove the feasibility of the proposed method.

This paper is arranged as follows. Section 2 introduces the basic principle of image identification with camera motion, including the correction of camera motion and drift detection based on the SfM method. Section 3 proves the proposed motion correction method by two shaking table tests with fewer and larger camera rotations. In Section 4, the displacement of a 3-story shaking table test is detected by the SfM method to verify the accuracy when applied to the real-scale multi-degree of freedom (MDOF) system. Conclusion is then drawn, and future research potential is discussed.

2. Methodology

The aim is to determine the deformation of the structure by distinguishing images at each time step and calculating the real-time drift ratio. As Figure 1 shows, for each time step t_i, this process involves three steps:

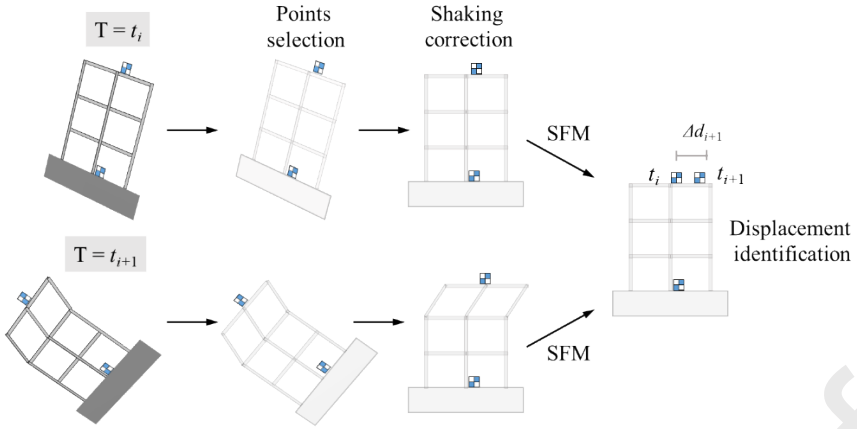

Figure 1. Basic description of image identification

1). Identification of coordinates of selected points. The reference points are selected from the attached signals. After that, projective correction is utilized to get rid of the influence of lens distortion;

2). Camera motion correction of identified coordinates. By fitting the points with the reference coordinates, the translation and rotation (both in and out of the plane) are identified and then utilized for calibration in this time step;

3). Displacement identification using the SfM method. The detailed methodology has been further clarified in this section.

The possible error during the drift detection mainly origin from the following parts:

1). Camera motion. The camera motion will give a huge change to the coordinate of the point in a figure.

2). Pixel identification. The identified accuracy is limited by the size of a pixel;

3). Assumption of rigid body. An SfM method assumes the coordinate of a part of the target will remain constant.

In this paper, the errors of 2) and 3) are ignored, and the main target is the correction of camera motion, which is clarified in detail below. Besides, though not fully discussed in this paper, the quantification of measuring uncertainty caused by the error is also a meaningful topic for the proposed observation method [31-32], which is expected to be carried out in the future.

2.1 Identification of coordinates

2.1.1 Point selection

The first step is to confirm the coordinates for the target structure. Considering the pictures taken by two cameras, there are three coordinate systems for the location identification of the target building. By translating the figures to the grey-scale map, a normal boundary recognition algorithm can identify all the points in the target structure in the two projected coordinate systems [33–35].

Since the story drift angle can be calculated by the relative displacement between the bottom and top floor, it is enough to use only two points to simplify the calculation. As shown in Figure 2, points A and B are set on the top and bottom floors. The calculated coordinates of the two points are a_1-b_1 and a_2-b_2, corresponding to the image taken by cameras 1 and 2. Considering the projective influence and the camera motion, the identified coordinates still need to be revised to achieve true coordinates A and B.

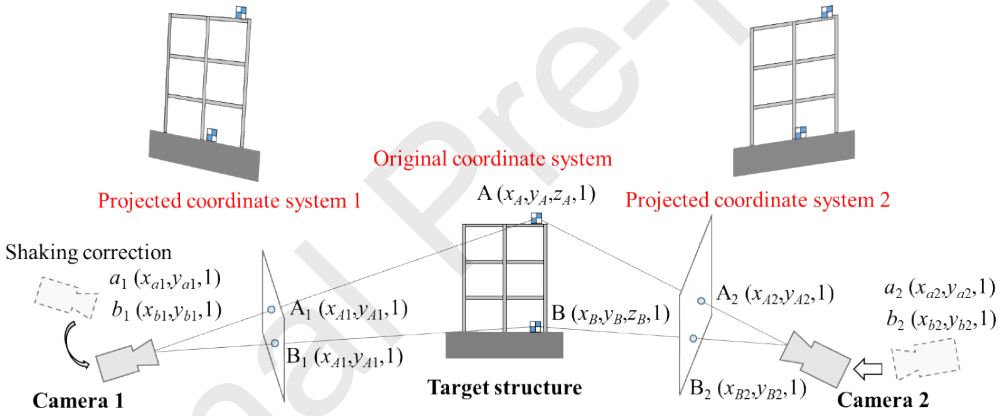

Figure 2. Points identification period

2.1.2 Projective correction

For each time step, the correct coordinates (A, B) can be obtained by correcting the projective. The back projection of point A can be shown as Equation 1.

$$\mathrm{A}_1 = P_1 \mathrm{A} \tag{1}$$

where A_1 is the coordinate of the points on the projected coordinate system 1 corresponding to point A. P_1 is the camera projection matrix of camera 1 containing all the transformation of coordinates, which is connected to the camera setting and location.

Considering the initial positional shift, the projection matrix P_1 can be shown as Equation 2.

$$P_1 = K_1[R_1|t_1] \tag{2}$$

where K_1 is the internal matrix controlling the transformation from 3D to 2D. R_1 and C_1 correspond to the transformational matrix of initial rotation and translation. Considering the photo center of camera 1 as the original coordinate system's original points, the values of the internal parameter matrix (K_1) and external parameter matrix (R_1 and t_1) are shown in Equation 3.

$$K_1 = \begin{bmatrix} a_{x1} & 0 & p_{x1} \\ 0 & a_{y1} & p_{y1} \\ 0 & 0 & 1 \end{bmatrix},\ R_1 = \begin{bmatrix} 1 & 0 & 0 \\ 0 & 1 & 0 \\ 0 & 0 & 1 \end{bmatrix},\ t_1 = -R_1C_1 = \begin{bmatrix} 0 \\ 0 \\ 0 \end{bmatrix} \tag{3}$$

where a_{x1}, a_{y1} are the focal length f transferred by the pixel density in the x and y direction (m_x and m_y), as shown in Equation 4.

$$a_{x1} = f \cdot m_x,\ a_{y1} = f \cdot m_y \tag{4}$$

By transferring the original point from the photo center of camera 1 to the reference point B on the structure, the external parameter matrixes R_1 and t_1 are rewritten as

$$R_1 = \begin{bmatrix} r_{11} & r_{12} & r_{13} \\ r_{14} & r_{15} & r_{16} \\ r_{17} & r_{18} & r_{19} \end{bmatrix},\ t_1 = -R_1C_1 = \begin{bmatrix} t_{11} \\ t_{12} \\ t_{13} \end{bmatrix}. \tag{5}$$

where r_{11}-r_{19} are the transfer parameters for rotation, and t_{11}-t_{13} are the parameters for translation.

Hence, when a camera's initial location and focal length are determined, the parameter matrixes K_1, R_1, and t_1 are decided, further determining the projection matrix P_1. Since the projection will reduce the information from 3D to 2D, at least 2 cameras are needed to solve the 3D coordinates of the target structure.

2.2 Shaking correction

If the camera is shaking during the video taking, the parameter matrixes will change continuously due to the location disturbing, where the correction of the parameter matrixes is needed. Hence, another external matrix is introduced to correct the influence of camera motions. The projection matrix $P_1^{'}$ is as follows:

$$P_1^{'} = K_1[R_{m1}|t_{m1}][R_1|t_1] \tag{6}$$

where R_{m1} and t_{m1} are the correction matrix of the motion of camera 1. Therefore, the influence can be corrected if the camera motion can be determined at each step.

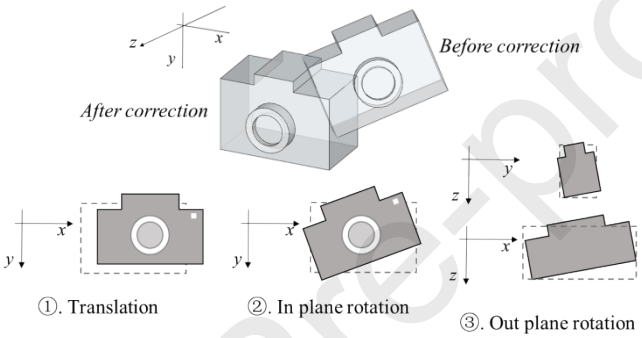

Figure 3. Type of shaking correction

As shown in Figure 3, the camera's shaking can be decomposed to the rotation (both in and out plane) and translational motion. Since the influences caused by these three effects are not coupled with each other, they have been revised separately in this Section. Besides, as the distance between the camera and the target structure is much bigger than the camera motion, changes in image size introduced by the camera motion are not considered.

2.2.1 Identification of fixed ground

The first thing for motion correction is to find a fixed ground of the target structure as a reference. For a normal SfM method, the fixed ground is identified from the boundary definition of the segmentation results. In this paper, two target points and two reference points are signed in advance, corresponding to the target structure and fixed ground, as Figure 4 shows. Generally speaking, the reference and target points are totally picked from the bottom and top of the target structure.

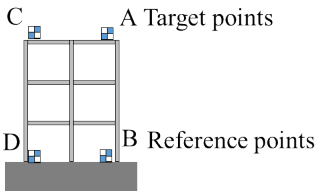

Figure 4. Target and reference points on the target structure

2.2.2 Correction of in-plane rotation

The camera rotation will introduce a global diversion. The influence can be compensated by subtracting the introduced diversion from the coordinates of each point. Assuming two reference points are fixed without any relative displacement, the angle of the connecting line is constant and hence taken as a conference. Defining the time before the earthquake happens as the initial state, the angle difference α between the reference line (initial state) and line at time t_i is selected as the camera rotation angle, as shown in Figure 5. Similar to the correction of the camera location, the influence of the rotation in the plane can be corrected as Equation 7.

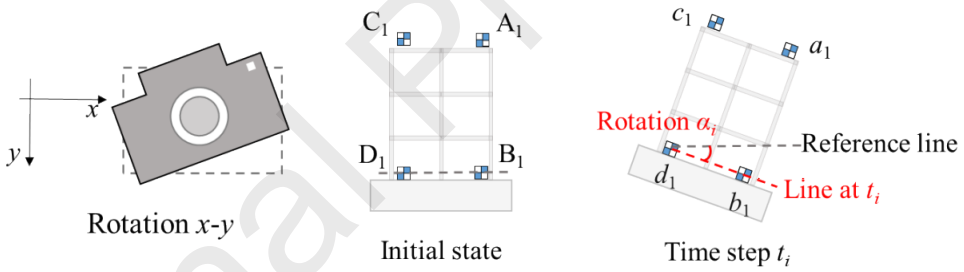

Figure 5. Correction of camera rotation in-plane

$$A_1 = R_z^{-1} a_1, \quad R_z = \begin{bmatrix} \cos\alpha & -\sin\alpha & 0 \\ \cos\alpha & \cos\alpha & 0 \\ 0 & 0 & 1 \end{bmatrix} \tag{7}$$

where R_z is the transfer matrix for the rotation in the x-y direction.

2.2.3 Correction of out-plane rotation

Similar to the in-plane rotation correction, the rotation out of the plane is corrected

by comparing the reference points before and after, as clarified in Figure 6. Taking point A as an example, the relationship between the coordinates of reference points and points at time t_i is shown in Equation 8.

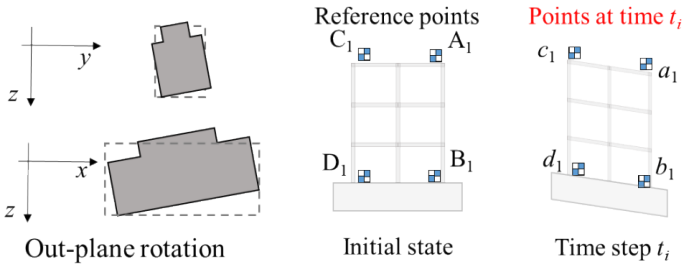

Figure 6. Correction of out-plane camera rotation

$$a_1 = R_x R_y \mathrm{A}_1 \tag{8}$$

where R_x and R_y defined in Equation 9 are the transfer matrix for the rotation in y-z and x-z directions.

$$R_x = \begin{bmatrix} 1 & 0 & 0 \\ 0 & \cos\beta & -\sin\beta \\ 0 & \sin\beta & \cos\beta \end{bmatrix}, \quad R_y = \begin{bmatrix} \cos\gamma & 0 & \sin\gamma \\ 0 & 1 & 0 \\ -\sin\gamma & 0 & \cos\gamma \end{bmatrix} \tag{9}$$

where β and γ are the rotation angles in the y-z and x-z directions, respectively.

Hence, by solving equation 8 using the coordinates of reference points and points at time t_i, β and γ can be calculated and further utilized to correct the rotation, as Equation 10 shows. It should be noted that points A and C can also be utilized for the calculation since the structure deformation is relatively small compared with the influence of camera motion.

$$\mathrm{A}_1 = R_x^{-1} R_y^{-1} a_1 \tag{10}$$

2.2.4 Correction of translational motion

Translational motion can be directly obtained from the coordinate difference between the reference points in the initial state and time t_i, as Figure 7 shows.

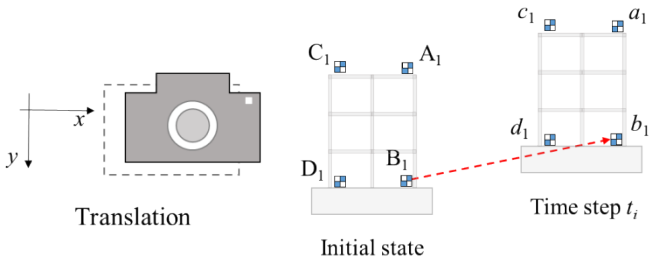

Figure 7. Correction of out-plane camera rotation

The correction of translational motion can then be revised using Equation 11

$$\mathrm{A}_1 = a_1 + R_t, \quad R_t = \begin{bmatrix} t_x \\ t_y \\ t_z \end{bmatrix} \tag{11}$$

where R_t is the transfer matrix for translational motion. t_x, t_y, and t_z correspond to the difference in the x, y, and z directions.

2.3 Detection of relative drift

2.3.1 Combination of motion correction and projective correction

Combining the projective correction in Section 2.1 and the motion correction in Section 2.2, the relationship between the projected (a_1) and real (A) coordinates is shown in Equation 12.

$$a_1 = P_1^{'}\mathrm{A}, \quad P_1^{'} = K_1[R_{m1}|R_t][R_1|t_1] \tag{12}$$

where R_{m1} and R_t can be calculated by Equation 13 based on Section 2.2

$$R_{m1} = R_x R_y R_z, \quad t_{m1} = \begin{bmatrix} t_x \\ t_y \\ t_z \end{bmatrix}. \tag{13}$$

2.3.2 Drift detection

For each time step t_i, the real coordinates (A_i) can be obtained based on Equation 12. The real-time drift can then be directly calculated from the difference of real coordinates of target points, as described in Equation 14 and Figure 8.

$$\Delta d_i = (A_i - A_0) \cdot m . \tag{14}$$

where Δd_i is the relative displacement at time t_i. m is the pixel density. A_0 and A_i are the real coordinates at initial time t_0 and time t_i.

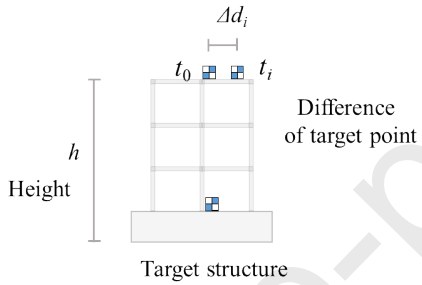

Figure 8. Drift detection

3. Experiments to confirm the motion correction method

The arrangement for the experiments in this Section is clarified in Table 1. Two cases are designed corresponding to the condition with a small or huge earthquake. A steel specimen shown in Figure 9 is utilized in both two cases. The basic parameters of the specimen, camera, and laser sensor have been listed in Table 2. The experiment setup and discussion of results are shown below.

Table 1 Arrangement of experiment

Case	Target condition	Camera motion	Section	Specimen	Detection
1	Small earthquake	translation(main), rotation(minor)	3.1	SDOF system	relative drift of 1F
2	Huge	Translation & rotation	3.2		

earthquake

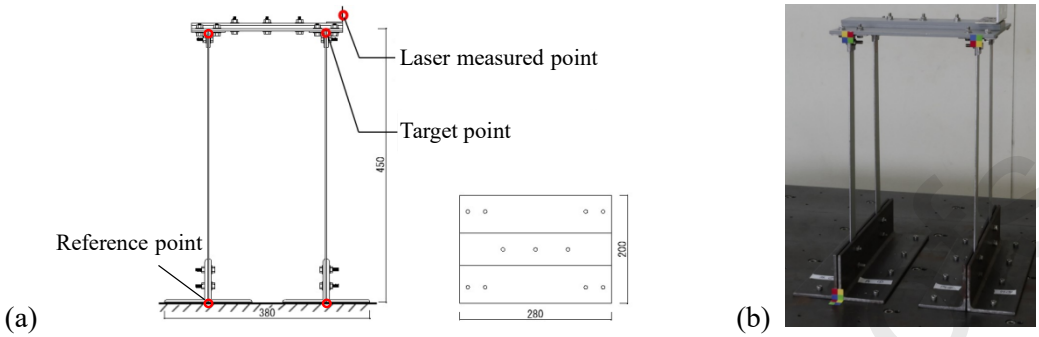

Figure 9. Utilized one-story scared specimen (a) Concept (b) real specimen

Table 2 Basic parameters of the utilized instruments

Instruments	Fabricator	Basic parameters
Camera	Canon EOSR5	Resolution: 8192×5464 Size: 138.5×97.5×88 (mm^3)
Laser sensor	KEYENCE LB 300	Resolution: 50μm Testing range: ±100 (mm) Size: 86×56×28 (mm^3)
Specimen	Own product	Material: steel Size: 450×380×200 (mm^3)

It should be noted that the dimensions of the instruments for observation will remain the same size as shown in Table 2 when applied to a real structure. Besides, the measured range of the real structure is determined by the size of the figure, which can

be adjusted by the camera setting and the distance between the camera and the real structure.

3.1 Camera motion with slight rotation

3.1.1 Experiment setup

The experiment is set as shown in Figure 10. The 1 story specimen mentioned above is bolted with the 1-direction shaking table. NS direction of the Hachinohe earthquake (1968) is selected to be the input ground motion [36]. Drifts of the specimen are detected by two systems. 1). A reference group is formed by two laser sensors attached to the right side of the shaking table. One on the upside is used to detect the 1F drift, and the other on the lower side is used for the ground motion. The drift from laser sensors is set as the reference group. 2). An SfM system as an experimental group is formed by two cameras bolted with a cantilever beam. Since the cantilever beam is not rigid, besides a similar motion with the shaking table, cameras will have slight extra translation and rotation caused by the shaking of the cantilever beam. At the corner of the specimen, a squared signal is attached as the target and reference points. The detected drift by the SfM system is then compared with the results by the laser sensors to confirm the feasibility of the proposed correction method of camera motion under a slight rotation case. The basic concept is further shown in Figure 11 as an experimental flow chart. To simplify the setting of the experiment, the cameras are directly placed in front of the specimen. It should be noted that the location of the cameras may also influence the accuracy of measurement, which will be discussed in the future [37].

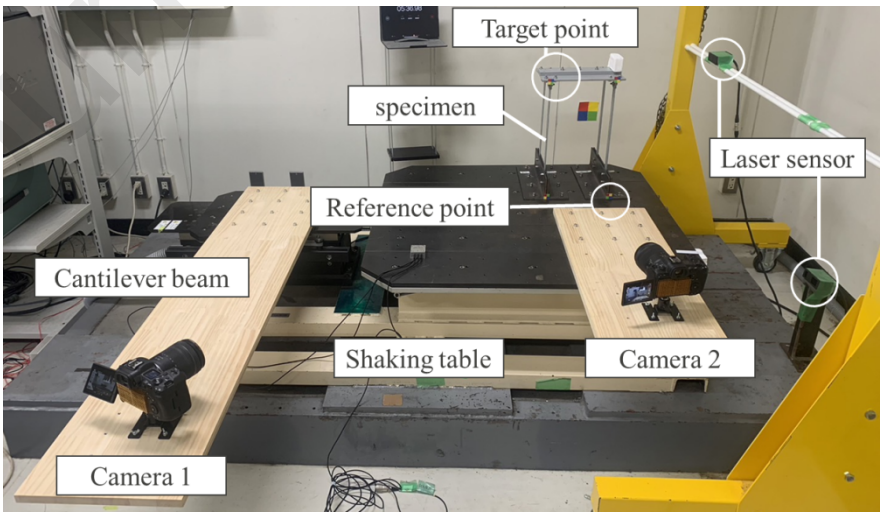

Figure 10. Experiment setup for case 1

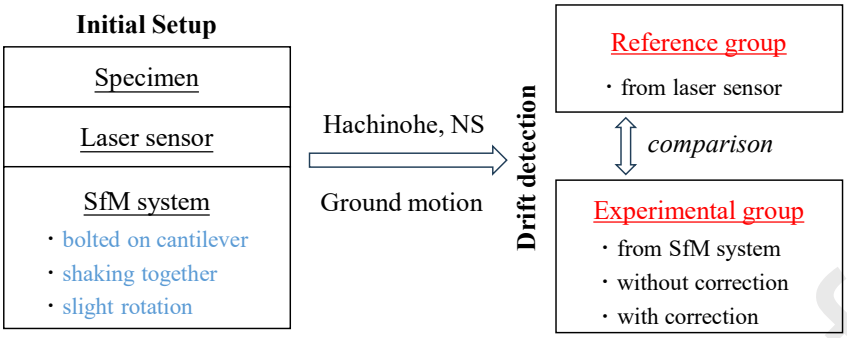

Figure 11. Flow chart of the experiment (Section 3 - case 1)

3.1.2 Result and discussion

As shown in Figure 12, there are three kinds of measured relative drifts, corresponding to results from the reference group (laser), and the results from the experimental group (SfM system) with & without correction of the camera motion. During the detection, the drift obtained from the reference group is regarded as an accurate value. Though a huge error exists in the experimental group without correction, it fits well with the reference group after correcting the camera motion. The slight error that existed in the results of the experimental group without correction may originate from the possible pixel error of the identified coordinate of each point and the fitting error for the rotation correction.

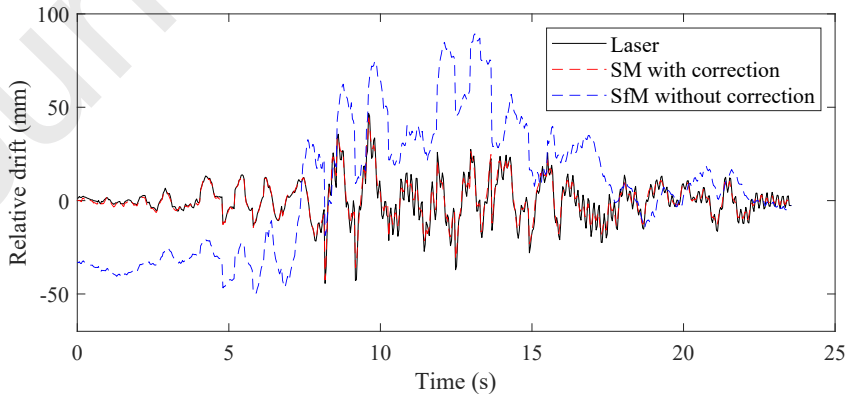

Figure 12. Identified story drift before and after correction of camera motion (case1)

Table 3 Calculated error for case 1 (%)

Parameter	Laser	Without correction	With correction
Value (mm)	46.7	89.3	44.3
R^2	/	0.021	0.944
Errror (%)	/	91.2	4.9

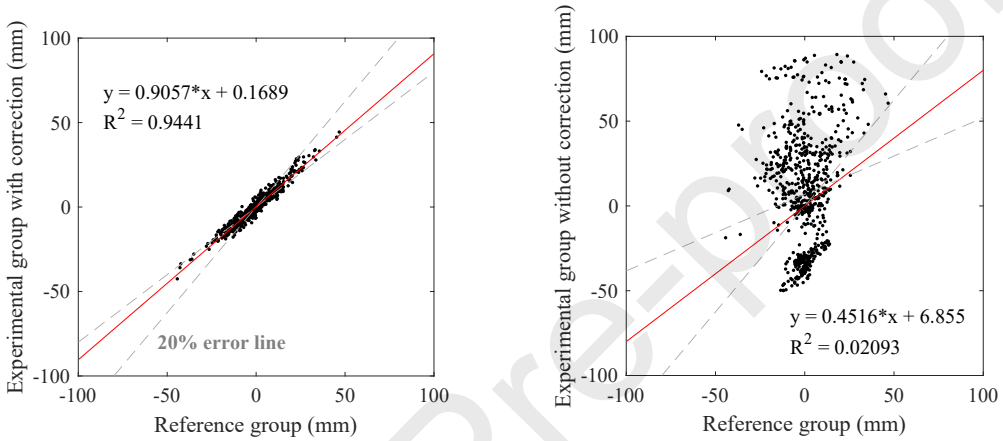

(a) (b)

Figure 13. Error evaluation of Case 1 (a) with correction (b) without correction

Error is then analyzed first by evaluating the dependency between the detected relative drift of the reference group and the experimental group, which is shown in Figure 13. After that, the error of the maximum absolute value of each group is shown in Table 3.

After correction of the camera motion, the linear fitting coefficient increases from 0.02 to 0.94, and the error of maximum absolute value reduces from 91.2% to 4.9%, which proves the feasibility of the proposed method for the correction of camera motion under case 1. It should be noted that the time of the detected drifts for reference and experimental groups is kept the same by fitting the measured peak values with each other. Hence, it may arouse possible errors. In the future, the synchronization error will be discussed when an SHM system is established using the camera and traditional sensors together as the next step.

3.2 Camera motion with larger rotation

3.2.1 Experiment setup

With the same instruments as shown in Table 1, the experiment is set as shown in Figure 14, and the basic concept is described in Figure 15 as an experimental flow chart. At this time, in order to introduce a larger rotation, a much more random camera motion has been introduced according to the experimenter's movement.

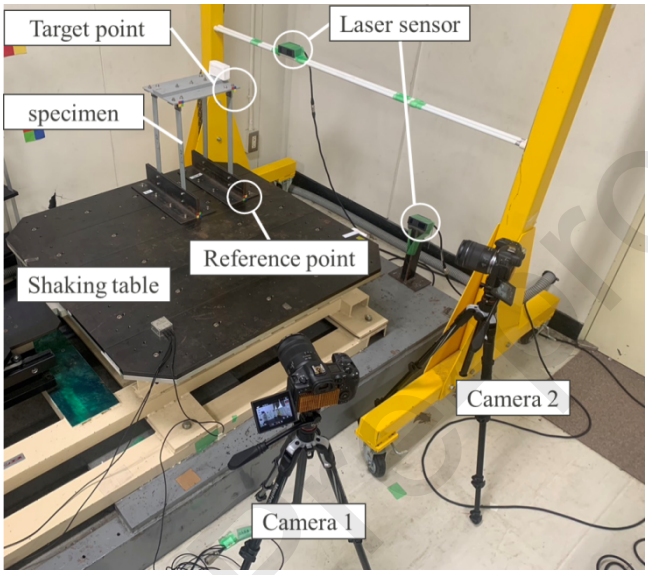

Figure 14. Experiment setup for case 2

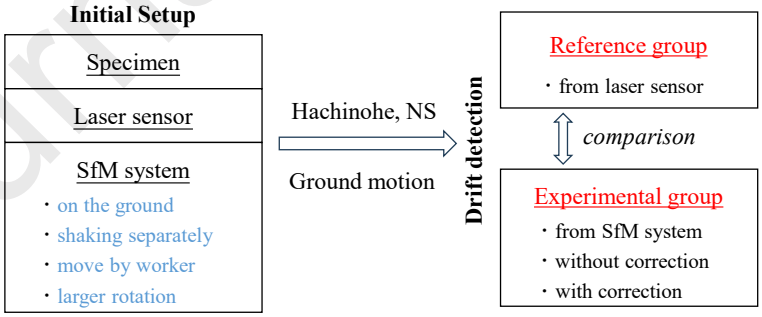

Figure 15. Flow chart of the experiment (Section 3 - case 2)

3.2.2 Result and Discussion

Similar to Section 3.1.2, the results for the reference and experimental groups have been shown in Figure 16. The correction of camera motion reduces the error.

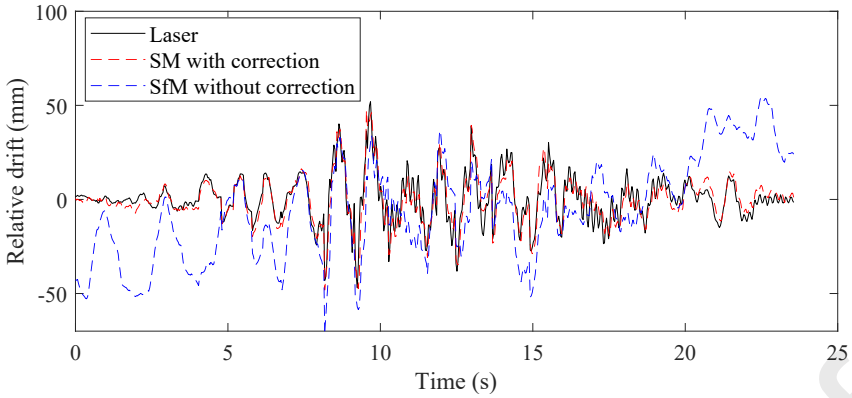

Figure 16. Identified story drift before and after correction of camera motion (case2)

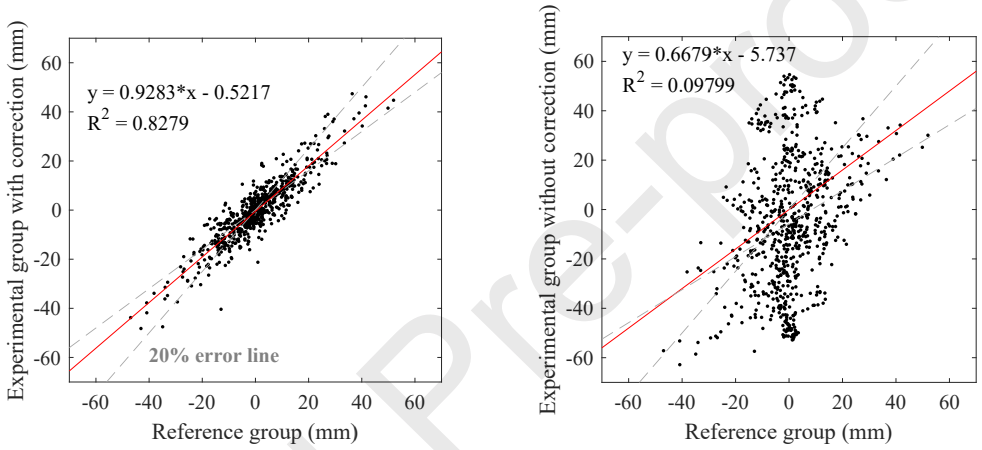

(a) (b)

Figure 17. Error evaluation of Case 2 (a) with correction (b) without correction

Table 4 Calculated error for case 2 (%)

Parameter	Laser	Without correction	With correction	With correction (case 1)
Value (mm)	51.9	70.4	48.2	/
R^2	/	0.098	0.828	0.944
Error (%)	/	37	7.3	4.9

Then, the same procedure is utilized in case 2, with the results shown in Figure 17 and Table 4. After the correction of the camera motion, the linear fitting coefficient increases from 0.09 to 0.83, and the error of maximum absolute value reduces from 37% to 7.3% under a signal-to-noise ratio of about -3dB, which proves the feasibility of the proposed method for the correction of camera motion under case 2.

However, it should be noted that compared with the error in case 1, the error increases from 4.9% to 7.3%, and the linear fitting coefficient decreases from 0.94 to 0.83, which indicates a huge influence on camera rotation. To ensure the feasibility of the proposed method under huge earthquakes with possible larger rotation, the method can still be updated.

4. Experiment to confirm the SfM method

4.1 Experiment setup

The SfM method is further applied in a 3-story shaking table test to confirm the real application's accuracy. The flow chart of the experiment is shown in Figure 18, with the setup shown in Figure 19. The drift of each floor has been measured by the laser sensor and the proposed image identification method based on the camera video records. Only the ability of the utilized SfM method is expected to be confirmed here. Hence, there is no camera motion during this measurement procedure.

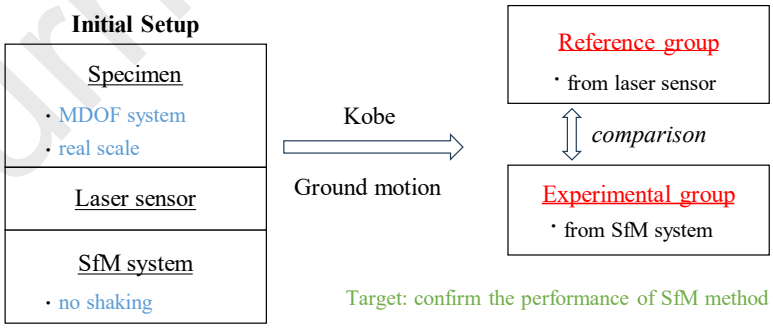

Figure 18. Flow chart of the experiment (Section 4)

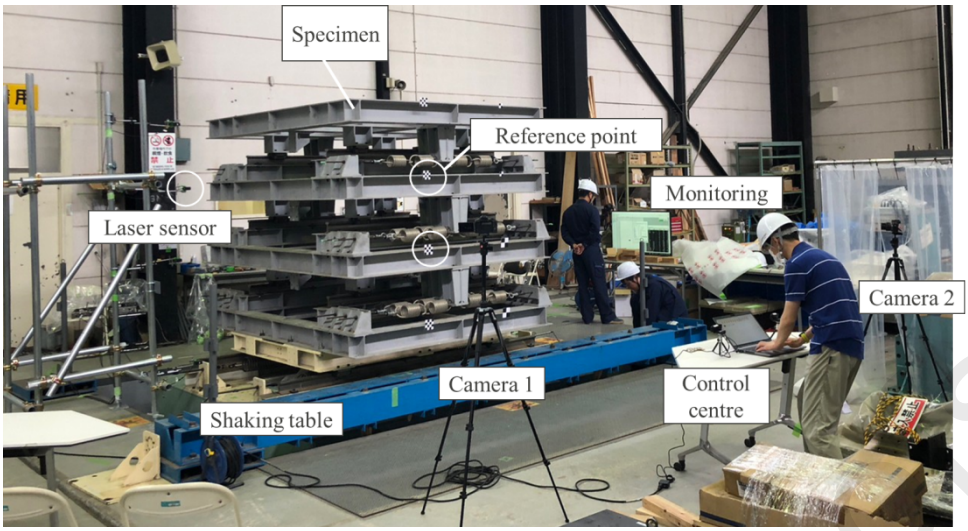

Figure 19. Setup of the experiment (3 stories shaking table experiment)

Kobe (1995) has been selected as the input ground motion in three directions. The same instruments, including the camera and laser sensor, have been applied to the experiment.

4.2 Result and Discussion

The measured displacement of floors 1 to 3 by the laser sensor and image-based identification method is plotted in Figure 20 and further compared in Figure 21. The two displacements can fit well in each case with a linear fitting coefficient over 0.9, which indicates that the SfM methods work well even for real-scared MDOF systems. However, the displacement from the camera shows a slight oscillation with a system error of about 1mm in the beginning and final parts, which should be noticed when the measured displacement is smaller than 10mm.

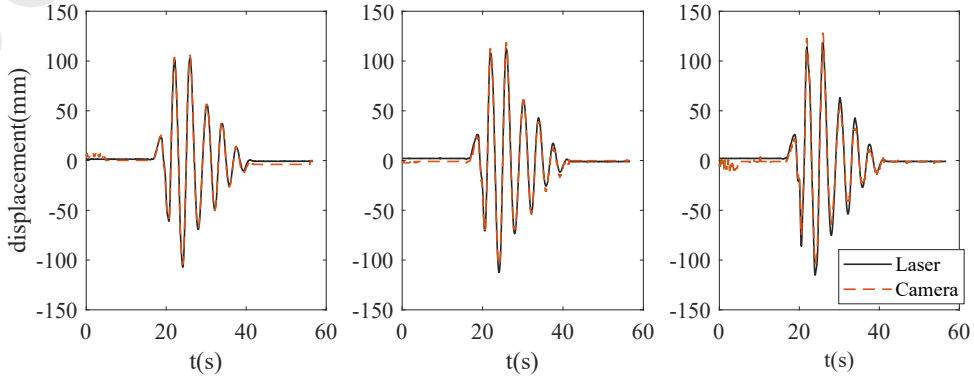

(a) 1F (b) 2F (c) 3F

Figure 20. Time domain of the identified relative displacement of each floor

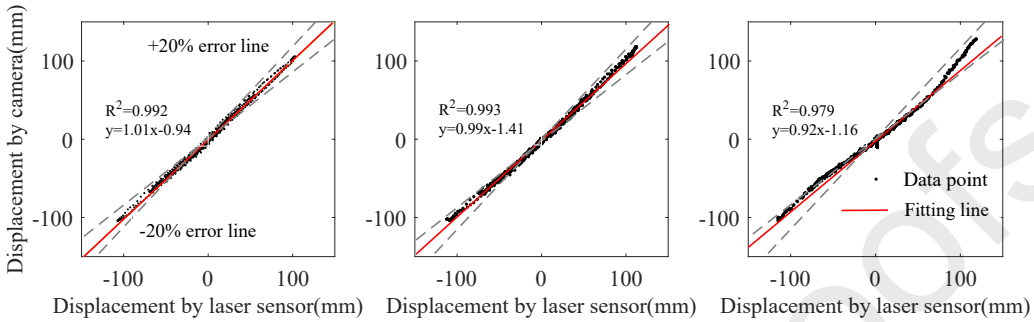

(a) 1F (b) 2F (c) 3F

Figure 21. Comparison of relative displacement of each floor from laser sensor and camera

Then, the maximum error has also been calculated and displayed in Table 5. Though the error slightly increases with the increase in displacement, all the computed errors are within 10%, which is suitable for practical utilization.

Table 5 Calculated error of relative story drift ratio (%)

Floor	1	2	3	Average (%)
Response_laser (mm)	107	112	119	/
Response_SfM (mm)	105	118	128	/
R^2	0.992	0.993	0.979	0.988
Error (%)	1.4	5.3	7.9	4.9

5. Conclusion

This paper has proposed a method for correcting camera motion in real-time displacement detection of target structures using camera video records. The proposed motion correction method has been verified using a scaled steel structure subjected to two different camera motions. After that, the ability of the SfM method is proved by an MDOF experiment. The following conclusions can be drawn based on this research:

1). After correction of the camera motion, the linear fitting coefficient increases from 0.02 to 0.94 for case 1 and from 0.09 to 0.83 for case 2, and the error of maximum absolute value reduces from 91% to 4.9% for case 1 and from 37% to 7.3%, which proves the feasibility of the proposed method for the correction of camera motion.

2). When the rotation of camera motion becomes more intense, the error increases from 4.9% to 7.3%, and the linear fitting coefficient decreases from 0.94 to 0.83, which indicates a huge influence on camera rotation. Nevertheless, the error still keeps relatively low, which means the proposed method is capable also under the case with large camera rotation.

3). An MDOF shaking table experiment has been utilized to confirm the feasibility of the proposed SfM method, and an average error of 4.9% for drift identification shows good applicability.

In the future, the following aspects are expected to be analyzed:

1). The influence of the camera location and the resolution of the video on the accuracy of measured drift.

2). The sensitivity and uncertainty of the proposed method.

3). The performance of the proposed method when utilized in the observation of real structures.

6. Acknowledgement

This research was supported by the Key Program of Intergovernmental International Scientific and Technological Innovation Cooperation (2021YFE0112200), the National Natural Science Foundation of China (Grant No. 51778490, 52178298), the Japan Society for Promotion of Science (Kakenhi No. 18K04438 and 21F21790). This work would like to thank Prof. Kohju Ikago for his kind help.

7. Reference

[1] P. Xiang, A. Nishitani, S. Marutani, K. Kodera, T. Hatada, R. Katamura, K. Kanekawa, T. Tanii, Identification of yield drift deformations and evaluation of the degree of damage through the direct sensing of drift displacements, *Earthq. Eng. Struct. Dyn*. 45 (2016) 2085–2102.

[2] C. Xiong, X. Lu, X. Lin, Damage assessment of shear wall components for RC frame–shear wall buildings using story curvature as engineering demand parameter, *Eng. Struct*. 189 (2019) 77–88.

[3] H.S. Park, H. Lee, H. Adeli, I. Lee, A new approach for health monitoring of structures: terrestrial laser scanning, *Comput. Civ. Infrastruct. Eng*. 22 (2007) 19–30.

[4] D. Feng, M.Q. Feng, Vision-based multipoint displacement measurement for structural health monitoring, *Struct. Control Health Monit*. 23 (2016) 876–890.

[5] K. Diamanti, C. Soutis, Structural health monitoring techniques for aircraft composite structures, *Prog. Aerosp. Sci.* 46 (2010) 342–352.

[6] A. Babu, B. George, Design and development of a new non-contact inductive displacement sensor, *IEEE Sens. J*. 18 (2017) 976–984.

[7] A. Drumea, M. Blejan, C. Ionescu, Differential inductive displacement sensor with integrated electronics and infrared communication capabilities, in: *Adv. Top. Optoelectron. Microelectron. Nanotechnologies* VI, SPIE, 2012: pp. 276–282.

[8] W. Li, J. Hu, Z. Su, D. Wang, Analysis and design of axial inductive displacement sensor, *Measurement*. 187 (2022) 110159.

[9] H.S. Park, H. Lee, H. Adeli, I. Lee, A new approach for health monitoring of structures: terrestrial laser scanning, *Comput. Civ. Infrastruct. Eng*. 22 (2007) 19–30.

[10] J. Sandak, C. Tanaka, Evaluation of surface smoothness by laser displacement sensor 1: Effect of wood species, *J. Wood Sci*. 49 (2003) 305–311.

[11] N. Servagent, T. Bosch, M. Lescure, A laser displacement sensor using the self-mixing effect for modal analysis and defect detection, *IEEE Trans. Instrum. Meas.* 46 (1997) 847–850.

[12] B. Sun, B. Li, Laser displacement sensor in the application of aero-engine blade measurement, *IEEE Sens. J*. 16 (2015) 1377–1384.

[13] H.F. Lima, R. da Silva Vicente, R.N. Nogueira, I. Abe, P.S. de Brito Andre, C. Fernandes, H.

Rodrigues, H. Varum, H.J. Kalinowski, A. Costa, Structural health monitoring of the church of Santa Casa da Misericórdia of Aveiro using FBG sensors, *IEEE Sens. J*. 8 (2008) 1236–1242.

[14] H. Iwaki, K. Shiba, N. Takeda, Structural health monitoring system using FBG-based sensors for a damage-tolerant building, in: *Smart Struct. Mater. 2003 Smart Syst. Nondestruct. Eval. Civ. Infrastruct.*, SPIE, 2003: pp. 392–399.

[15] H. Mandal, S.K. Bera, S. Saha, P.K. Sadhu, S.C. Bera, Study of a modified LVDT type displacement transducer with unlimited range, *IEEE Sens. J*. 18 (2018) 9501–9514.

[16] S.-T. Wu, S.-C. Mo, B.-S. Wu, An LVDT-based self-actuating displacement transducer, *Sens. Actuators Phys*. 141 (2008) 558–564.

[17] Y.K. Thong, M.S. Woolfson, J.A. Crowe, B.R. Hayes-Gill, D.A. Jones, Numerical double integration of acceleration measurements in noise, *Measurement*. 36 (2004) 73–92.

[18] J.G.T. Ribeiro, J.T.P. de Castro, M.A. Meggiolaro, An algorithm to minimize errors in displacement measurements via double integration of noisy acceleration signals, *J. Braz. Soc. Mech. Sci. Eng*. 43 (2021) 1–21.

[19] M.P. Limongelli, Frequency response function interpolation for damage detection under changing environment, *Mech. Syst. Signal Process*. 24 (2010) 2898–2913.

[20] M.-B. Abdo, M. Hori, A numerical study of structural damage detection using changes in the rotation of mode shapes, *J. Sound Vib*. 251 (2002) 227–239.

[21] Y. Lei, D. Xia, K. Erazo, S. Nagarajaiah, A novel unscented Kalman filter for recursive state-input-system identification of nonlinear systems, *Mech. Syst. Signal Process*. 127 (2019) 120–135.

[22] R. Astroza, H. Ebrahimian, Y. Li, J.P. Conte, Bayesian nonlinear structural FE model and seismic input identification for damage assessment of civil structures, *Mech. Syst. Signal Process*. 93 (2017) 661–687.

[23] Spencer Jr, Billie. F, Vedhus. Hoskere, and Yasutaka. Narazaki. Advances in computer vision-based civil infrastructure inspection and monitoring. *Engineering.* 5.2 (2019) 199-222.

[24] Kassotakis, N., Sarhosis, V., Peppa, M. V., & Mills, J. Quantifying the effect of geometric uncertainty on the structural behaviour of arches developed from direct measurement and Structure-from-Motion (SfM) photogrammetry. *Eng. Struct*., 230, (2021) 111710.

[25] Wang, Tuanfeng Y., Pushmeet Kohli, and Niloy J. Mitra. Dynamic SFM: detecting scene changes from image pairs. In *Computer Graphics Forum*, 34 (5), (2015) 177-189.

[26] Wang, X., Wittich, C. E., Hutchinson, T. C., Bock, Y., Goldberg, D., Lo, E., & Kuester, F. Methodology and validation of UAV-based video analysis approach for tracking earthquake-induced building displacements. *J. Comput. Civil. Eng.*, 34(6), (2020). 04020045.

[27] J. Kim, Y. Jeong, H. Lee, H. Yun, Marker-based structural displacement measurement models with camera movement error correction using image matching and anomaly detection, *Sensors*. 20 (2020) 5676.

[28] J. Jiao, J. Guo, K. Fujita, I. Takewaki, Displacement measurement and nonlinear structural system identification: a vision-based approach with camera motion correction using planar structures, *Struct. Control Health Monit*. 28 (2021) e2761.

[29] Shao, Xinxing, and Xiaoyuan He. Camera motion-induced systematic errors in stereo-DIC and speckle-based compensation method. *Opt. Lasers Eng.* 149 (2022), 106809.

[30] Zhao, Chunhui, Yakun Li, and Yang Lyu. "Event-based Real-time Moving Object Detection Based On IMU Ego-motion Compensation." In *2023 IEEE International Conference on Robotics and Automation (ICRA)*, IEEE, (2023). 690-696.

[31] C. Yang, Interval strategy-based regularization approach for force reconstruction with multi-source uncertainties, *Comput. Meth. Appl. Mech. Eng*. 419 (2024): 116679.

[32] C Yang, Y Xia, Interval Pareto front-based multi-objective robust optimization for sensor placement in structural modal identification. *Reliab. Eng. Syst. Saf*. 242 (2024): 109703.

[33] G. Han, J. Shen, L. Liu, L. Shu, BRTCO: A novel boundary recognition and tracking algorithm for continuous objects in wireless sensor networks, *IEEE Syst. J*. 12 (2016) 2056–2065.

[34] G.-D. Wu, C.-T. Lin, Word boundary detection with mel-scale frequency bank in noisy environment, *IEEE Trans. Speech Audio Process*. 8 (2000) 541–554.

[35] Y. Yakimovsky, Boundary and object detection in real world images, *J. ACM*. 23 (1976) 599–618.

[36] Japanese Strong-motion Seismograph Networks (K-NET, KiK-net), https://www.kyoshin.bosai.go.jp/.

[37] C Yang, K Liang, X Zhang, X Geng: Sensor placement algorithm for structural health

monitoring with redundancy elimination model based on sub-clustering strategy. *Mechanical Systems and Signal Processing*, 124(2019), 369-387.

Highlight:

・Motion correction method is proposed to deal with real-time camera motion in all directions during the structural drift identification using SFM method.

・Motion correction method is verified by two single-degree-of-freedom experiments with slight and huge rotation.

・Error of identified maximum drift decreased to 7.3% after correcting camera motion.

・SFM method is verified by a multi-degree-of-freedom experiment with an average error of 4.5%.

Declaration of interests

☒ The authors declare that they have no known competing financial interests or personal relationships that could have appeared to influence the work reported in this paper.

☐ The authors declare the following financial interests/personal relationships which may be considered as potential competing interests: